View metadata, citation and similar papers at core.ac.uk

brought to you by CORE

provided by Institutionelles Repositorium der Leibniz Universität Hannover

Journal of The Electrochemical Society

The Electrochemical Society
Advancing solid state & electrochemical science & technology

OPEN ACCESS

Elucidating the Effect of Mass Transport Resistances on Hydrogen Crossover and Cell Performance in PEM Water Electrolyzers by Varying the Cathode Ionomer Content

To cite this article: P. Trinke *et al* 2019 *J. Electrochem. Soc.* **166** F465

View the article online for updates and enhancements.

This content was downloaded from IP address 194.95.157.39 on 05/11/2020 at 10:22

Elucidating the Effect of Mass Transport Resistances on Hydrogen Crossover and Cell Performance in PEM Water Electrolyzers by Varying the Cathode Ionomer Content

P. Trinke,[1] G. P. Keeley,[2] M. Carmo,[2] B. Bensmann,[1,z] and R. Hanke-Rauschenbach[1]

[1] *Institute of Electric Power Systems, Leibniz Universität Hannover, 30167 Hannover, Germany*
[2] *Forschungszentrum Jülich GmbH, Institute of Energy and Climate Research, IEK-3: Electrochemical Process Engineering, 52425 Jülich, Germany*

An important challenge for polymer electrolyte membrane (PEM) water electrolysis is to reduce the permeation of the produced gases. This crossover affects the cell efficiency and causes safety issues. The crossover increases with current density, most probably due to mass transfer resistances. This work aims to investigate the influence of the cathode ionomer content on hydrogen crossover. Therefore, the ionomer content was varied between 10 and 40 wt% to clearly influence the mass transfer resistances. The best performance and lowest crossover was obtained for 10 wt% ionomer. However, within the observed ionomer range the mass transfer resistances increase with ionomer content that cause increases in hydrogen crossover and cell voltage. Both can be entirely explained by the same quantity of supersaturated dissolved hydrogen concentrations. These supersaturated concentrations cause higher cathode half-cell potentials, which explain the cell voltage increase and lead to higher concentration gradients across the membrane, which enhance the crossover. These findings highlight the importance of mass transfer resistances within catalyst layers in terms of crossover and performance. They constitute an important step in the clarification of the complex interplay between mass transport and voltage losses, enabling the development of novel electrode architectures for PEM water electrolyzers.
© The Author(s) 2019. Published by ECS. This is an open access article distributed under the terms of the Creative Commons Attribution 4.0 License (CC BY, http://creativecommons.org/licenses/by/4.0/), which permits unrestricted reuse of the work in any medium, provided the original work is properly cited. [DOI: 10.1149/2.0171908jes]

Manuscript submitted November 25, 2018; revised manuscript received February 27, 2019. Published April 25, 2019.

Prevention of gas crossover in polymer electrolyte membrane (PEM) water electrolyzers constitutes an important objective. It causes safety[1–4] and degradation[5] issues and makes up relevant Faraday losses.[1,2] Therefore, it has gained increasing attention in scientific research.

Gas crossover mainly occurs within the aqueous phase of the PEM.[4,6,7] The driving force of the diffusive transport process is the difference of dissolved gas concentrations in the liquid water phases across the membrane.[4,6,7] Under normal electrolysis conditions, in which the PEM electrolysis cell is flooded, this crossover is obviously affected by operating pressure[3,4,7–10] and temperature,[3,7–11] either increasing the dissolved gas concentration or the permeability.

More recently are the findings related to the strong dependence of crossover on current density. A linear increase of hydrogen crossover flux with current density was revealed by Trinke et al.[3] in a current density range of 0.05 to 1 A cm^{-2}. In addition to this experimental finding, they recalculated data from previous hydrogen in oxygen measurements from Grigoriev et al.[1] and Schalenbach et al.[2] to show that this effect appears also for other systems. It has also been shown that the oxygen crossover exhibits the same trend.[12]

It was suggested, that this increase of crossover with current density is related to an increase of the dissolved gas concentrations within the catalyst layers above the saturation concentrations due to mass transfer resistances.[3] So, this supersaturation leads to higher concentration gradients across the membrane that cause increases in crossover. Such supersaturations have already been measured for electrolysis conditions.[13–15]

However, the impact of this crossover increase with current density depends on operating parameters and test equipment. It was shown that cathode pressures and cell temperatures cause slight differences,[3] whereas measurements at balanced pressure do not differ from those with differential pressure.[2,4]

However, the slope of the crossover increase strongly differs within the literature.[3] Since the supersaturation is caused by mass transfer resistances within the catalyst layers, it has been suggested that these differences are mainly caused by the different applied materials with different transport properties.[3]

Hegge et al.[16] analyzed the structure of a PEM water electrolysis anode catalyst layer by performing FIB-SEM tomography and subsequently modeling of different ionomer contents. It was shown that several mass transport properties such as pore space, relative permeability and the mean path length of the catalyst surrounding ionomer film change strongly with ionomer content. Consequently, variation in ionomer content should influence the supersaturation within the catalyst layer and thus should affect the crossover.

With this in mind various cathode catalyst layers with different ionomer contents were employed in this work to investigate the effect of different mass transfer resistances on hydrogen crossover. For this analysis the hydrogen in oxygen content of the anodic product gas was measured. Additionally, cell performance was recorded by using polarization curves with simultaneous measurement of the high frequency resistance.

Materials and Methods

CCM Preparation.—Fig. 1 shows the preparation process of the catalyst-coated membranes (CCMs) used in this work that were fabricated using a doctor-blade and decal method to transfer suitable cathode layers onto commercially available (HIAT gGmbH), half-coated (anode side only) membranes. The latter consisted of layers of iridium black (2 $mg_{Ir}cm^{-2}$, active geometric area 25 cm^2) coated onto N115 membranes. These commercial half-coated membranes were used to provide reproducible anodes, since in this communication only the influence of different cathodes is investigated.

To prepare the transferable cathodes, 60% Pt/C (HiSPEC 9100, Johnson & Matthey) and various amounts of ionomer solution (LQ 1115 15 wt% Nafion) were dispersed in a mixture of water, organic solvent, as well as an organic additive in cylindrical glass containers. The mixtures were homogenized in an ultrasonic device (Bandelin HD3200) for 2–10 min and then deposited on inert decal substrates using automated bar coating (Coatmaster 509 MCI, Erichsen GmbH & Co. KG). The bare sides of the commercially available half-CCMs were cleaned, and the dried cathode layers were hot-pressed on at a temperature of 150°C for around 10–15 min. The final cathode loadings were about 0.8 mg_{Pt} cm^{-2}.

Measurement devices.—The electrochemical measurements were carried out at a Greenlight E100 test station. Deionized water feed for the anode was set to 50 g min^{-1} and the inlet temperature to 80°C at ambient pressure conditions. The gas water mixtures were separated in two steps with an intermediate cooling process of the gases. For

[z] E-mail: boris.bensmann@ifes.uni-hannover.de

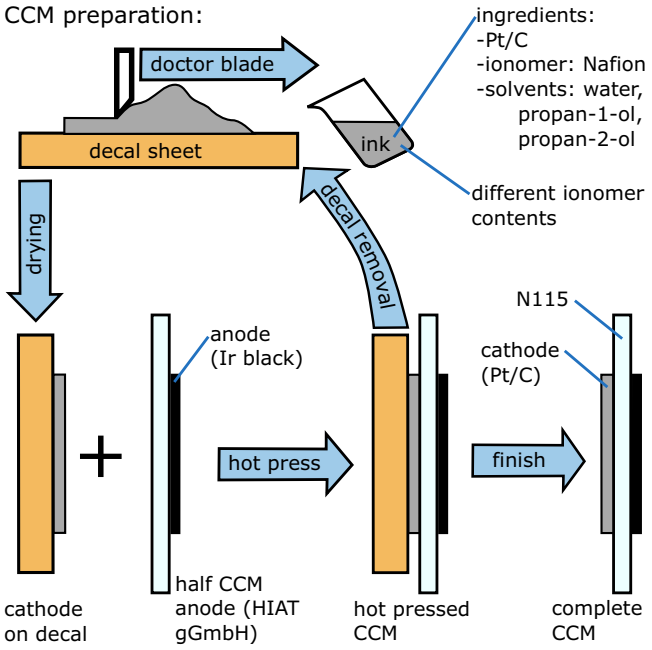

Figure 1. Scheme of the CCM preparation process.

the hydrogen in oxygen measurement the current was supplied by an Ametek Sorensen XG 6-220 power supply (±0.2% of reading). While the performance measurements were carried out with the electrochemical test system ModuLab XM ECS.

Cell.—The CCMs were inserted into a liquid cooled quick connect system (baltic FuelCells GmbH) with a 25 cm^2 cell insert, equipped with gold coated parallel flow fields. Cell temperature was maintained to 80°C by a circulation thermostat. The clamping pressure on the active area was set to 1.4 MPa by applying a nitrogen pressure of 4.5 bar to the piston.

Sintered titanium fibers with diameters of 20 µm, porosity of 0.56 and thickness of 1 mm (2GDL40-1,00, Bekaert) and a Toray carbon paper with a porosity of 0.78 and a thickness of 370 µm (TGP-H-120) were used as porous transport layers on the anode and cathode side, respectively.

Gas chromatograph.—For the measurement of the hydrogen in oxygen content an Agilent 490 gas chromatograph (GC) was used. The micro-GC took every 3 minutes a sample of the anode gas of the test station outlet. The oxygen hydrogen mixture was separated with a 10 m long 5 Å molecular sieve column and analyzed by a thermal conductivity detector. For calibration of the micro-GC 4 different test gas mixtures of 0.1, 1 and 2.5 wt% hydrogen in oxygen and 10 wt% hydrogen in nitrogen (±2% of reading, Linde) were used.

Electrochemical test system.—Polarization curves, electrochemical impedance spectroscopy (EIS) and high frequency resistance (HFR) were measured by a ModuLab XM ECS (Solartron analytical). The ModuLab was equipped with a XM FRA card, a XM PSTAT card and an external 100 A booster.

Methods.—*Performance.*—Polarization curves were measured galvanostatically with logarithmic steps from 0.01 to 1 A cm^{-2} and a constant step size of 0.1 A cm^{-2} between 1 and 2 A cm^{-2}. Each step was held for 10 s with a sample rate of 5 Hz. The last 5 measured values of each step were averaged for the polarization curves.

Between each galvanostatic step the HFR was measured. Therefore, short galvanostatic EIS measurements were implemented with sinusoidal current density signals with frequencies from 50 to 0.1 kHz and a root mean square of 10% of the applied DC current. The area-normalized HFR was determined as the impedance values at a phase angle of 0° multiplied by the active area.

EIS.—Galvanostatic EIS measurements were conducted at several DC current densities from 0.05 to 2 A cm^{-2}. The frequencies of the sinus signal were changed from 100 kHz to 0.1 Hz with a root mean square of 10% of the DC current.

Hydrogen content and crossover.—The H_2 in O_2 content was measured every three minutes with the micro-GC for 8 different current densities from 0.1 to 2 A cm^{-2}. Each current step was held for several hours until the hydrogen content reached a steady state. At low current densities more time is necessary to reach the steady state compared to higher current densities, because of the low gas production rates.

The hydrogen crossover $N_{H_2}^{cross}$ can be calculated by Eq. 1, assuming that no hydrogen oxidizes at the anode, the analyzed anodic product gas is dry and can be considered as an ideal gas as well as that the oxygen crossover can be neglected.[3]

$$N_{H_2}^{cross} = \frac{i}{4F}\frac{\phi_{H_2}}{1-\phi_{H_2}} \quad [1]$$

Where i is the applied current density, F the Faraday constant and ϕ_{H_2} the measured hydrogen in oxygen volume fraction.

Imaging.—For cross-section imaging, a strip of the dried CCM was embedded in epoxy resin and polished. Images were recorded using a Carl Zeiss SEM Gemini Ultra Plus. To determine the elemental distribution across each cathode layer, EDS line-scans were performed across the layer thickness with a SiLi detector from Oxford Instrument Pentex FET.

For each CCM, approximately 10 EDS line-scans were taken inside of the cathode electrodes to investigate if there were inhomogeneities. All EDs line scans were averaged to determine the mean weight percentage of fluorine of the different cathode catalyst layers and for the membrane.

Results and Discussion

Cathode ionomer variation.—Fig. 2 shows SEM cross sections and element mapping of platinum and fluorine of the four different cathode catalyst layers with varied ionomer content. The SEM/EDS measurements were performed after the electrochemical characterization. The cathode catalyst layers are relatively thick (≈23–25 µm), but there are no significant differences in the electrode thickness. This was also shown by Bernt and Gasteiger[17] for electrolyzer anodes, when varying the ionomer content within the anode catalyst layer.

The element mapping of Pt and F lead to the assumptions that the catalyst and the fluorine containing ionomer are quite homogeneously distributed within the cathode catalyst layers. The average weight percentages of fluorine within the different cathode catalyst layers show that the ionomer content was successfully varied by the cathode catalyst manufacturing.

Before the cathode catalyst layers were investigated by SEM/EDS imaging, the full CCMs were characterized in terms of electrochemical performance and hydrogen crossover, which is shown and described within the following subsections.

Effect on hydrogen crossover.—Fig. 3 shows the results of the hydrogen crossover investigation. In Fig. 3a the measured H_2 in O_2 content is plotted against current density. It can be seen that the H_2 in O_2 content is larger for the CCMs with higher ionomer contents. Despite the fact that these measurements were performed at atmospheric pressure conditions and with relatively thick N115 membranes the H_2 in O_2 contents are very high for the CCMs with 30 and 40 wt% ionomer, around 1 and 2 vol.% at 2 A cm^{-2}, respectively. So, there is a clear strong influence of high cathode ionomer loadings on the H_2 in O_2 content.

The corresponding hydrogen crossover flux is shown in Fig. 3b. It was calculated by Eq. 1 from the measured H_2 in O_2 content of

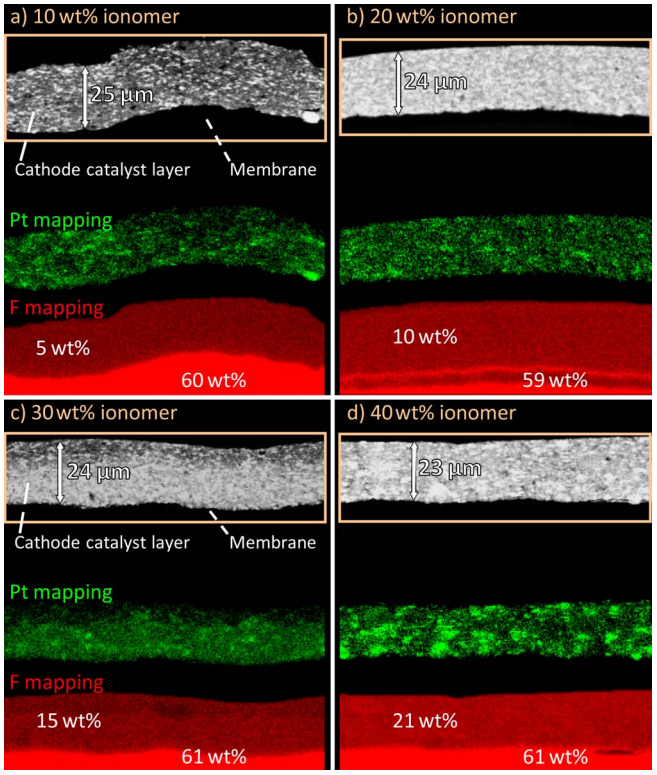

Figure 2. SEM cross sections of the cathode catalyst layers with varied ionomer content. Element mapping of platinum (green) and fluorine (red) are shown below the SEM images. The weight percentages for the fluorine content are averaged values for the catalyst layer and membrane.

Fig. 3a. Fig. 3b shows that the hydrogen crossover increases with increasing current density for all ionomer contents. However, the slopes are significantly higher for the CCMs with higher ionomer contents. Nevertheless, all four CCMs seem to have similar y-axis intersections. This behavior was expected, since the y-axis intersection (zero applied current) should be equal to the hydrogen crossover at saturated conditions.[3] Hence, the intersection should be equal for all CCMs, since they all consist of N115 membranes and were characterized under the same operating conditions (e.g. temperature, pressure).

The dashed lines of Fig. 3b represent the hydrogen crossover that is fitted to the experimental results by using Eqs. 2 and 3. Fick's first law, Eq. 2, is used to calculate the hydrogen crossover through the membrane. Therefore, the low hydrogen concentration of the anode is neglected. The supersaturated hydrogen concentration $c^{\star}_{H_2}$ of the cathode can be calculated out of the cathodic mass balance Eq. 3.[3]

$$N^{\text{cross}}_{H_2} = D^{\text{mem}}_{H_2} \frac{c^{\star}_{H_2} - \cancel{c^{a}_{H_2}}^{\,0}}{\delta^{\text{mem}}} \qquad [2]$$

$$c^{\star}_{H_2} : 0 = \underbrace{\frac{i}{2F}}_{H_2 \text{ evolution}} - \underbrace{D^{\text{mem}}_{H_2} \frac{c^{\star}_{H_2} - \cancel{c^{a}_{H_2}}^{\,0}}{\delta^{\text{mem}}}}_{H_2 \text{ transport through mem}} - \underbrace{k^{c}_{l}\left(c^{\star}_{H_2} - c^{\text{sat}}_{H_2}\right)}_{H_2 \text{ transfer toward the gas phase}} \qquad [3]$$

Where $c^{\star}_{H_2}$ is the supersaturated hydrogen concentration within the cathode catalyst layer, $c^{\text{sat}}_{H_2}$ is the saturated hydrogen concentration, δ^{mem} is the membrane thickness and $D^{\text{mem}}_{H_2}$ is the hydrogen diffusion coefficient of the humidified membrane. Parameter values are given in Table I. The single fitting parameter is the cathodic mass transfer coefficient k^{c}_{l} within the cathodic mass balance that was determined for each of the specific cathode catalyst layers separately.

The fitted crossover data with the determined cathodic mass transfer coefficient k^{c}_{l} agrees quite well to the experimental results. It was

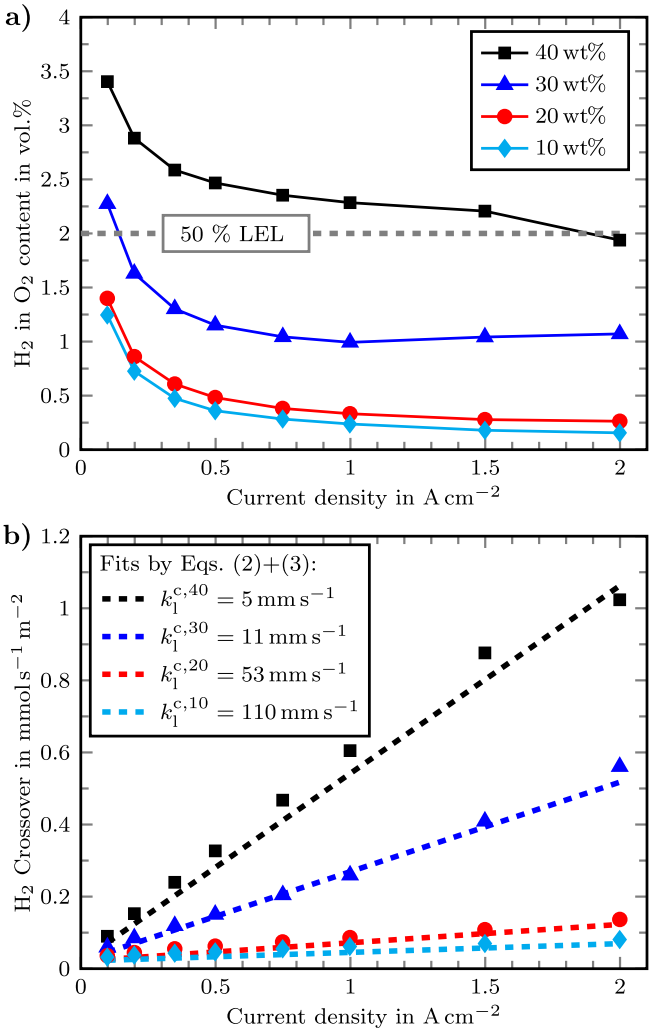

Figure 3. Subfigure a) shows the measured H_2 in O_2 content and b) shows the H_2 crossover vs. current density. The dashed lines of b) were fitted by Eqs. 2 and 3 with the parameters of Table I. The single fitting parameter is the cathode mass transfer coefficient k^{c}_{l}, which is stated for each cathode catalyst layer in the text box.

found to be between 5 and 110 mm s^{-1} for the 40 wt% and 10 wt% CCM, respectively. These results agree with the reported literature value of 3 mm s^{-1} for a fumea EF-40 CCM and with the finding that the mass transfer coefficient can be also up to one order of magnitude higher.[3] The cathode mass transfer coefficient determined in this work decreases with increasing cathodic ionomer content, which means that the mass transfer resistance increases with ionomer content. An explanation of this might result from structural changes within the catalyst layers. The following three properties are influenced if the ionomer content is increased:

i) decrease in hydraulic permeability: influenced by the decreasing pore space and increasing tortuosity of the pore volume. This hinders the hydraulic gas transport within the pore space.
ii) increase in ionomer film thickness: more ionomer results in longer pathways for the diffusive transport of produced dissolved hydrogen from the catalyst particles toward the pore space.
iii) decrease in volume specific surface of the pores: this reduces the interface between ionomer and pore space, which reduces the transfer of dissolved gas toward the gas state.

So, the mass transfer resistance of produced dissolved hydrogen toward the pore space of the catalyst layer is increased with increasing

Table I. The operating conditions and necessary parameter values for Eqs. 2 and 3.

Parameter	values at $T = 80°C$
Membrane thickness δ^{mem}	125 µm
Hydrogen solubility S_{H_2}	$7.6 \cdot 10^{-6}$ molPa^{-1} m^{-3}[18]
Diffusion coefficient D_{H_2}	$6.9 \cdot 10^{-9}$ m^2 s^{-1}[16]
Membrane water fraction $\varepsilon^{mem}_{H_2O}$	0.42[19]
Effective diffusion coefficient: $D^{mem}_{H_2} = \varepsilon^{mem}_{H_2O} D_{H_2}$	$2.9 \cdot 10^{-9}$ m^2 s^{-1}
Cathode pressure p^c	$1 \cdot 10^5$ Pa
Saturated vapor pressure $p^{sat}_{H_2O}$	$0.47 \cdot 10^5$ Pa[20]
Partial hydrogen pressure: $p_{H_2} = p^c - p^{sat}_{H_2O}$	$0.53 \cdot 10^5$ Pa
Saturated hydrogen conc.: $c^{sat}_{H_2} = p_{H_2} S_{H_2}$	0.36 mol m^{-3}

ionomer content. This is attributed to the reduction in pore space, by filling with ionomer. The resulting decrease in pore space, longer ionomer pathways and less available interfaces hinders the transfer of dissolved gas out of the catalyst layer. These three points were recently shown by use of FIB-SEM tomography of a PEM electrolyzer anode and modeling of various ionomoer contents by Hegge et al.[16]

The supersaturated dissolved hydrogen concentration $c^{\star}_{H_2}$ of the cathode catalyst layers follows from Eq. 3 and is shown in Fig. 4. Additionally, the saturated dissolved hydrogen concentration is plotted, which is around 0.36 mol m^{-3} at atmospheric cathode pressure and 80°C. Fig. 4 shows that the calculated dissolved hydrogen concentration during PEM water electrolysis is several times higher than the saturated concentration. For the 40 wt% CCM at 2 A cm^{-2} the concentration is more than 50 times higher than the saturation concentration, whereas for the 10 wt% CCM it is only 5 times higher. However, each CCM shows supersaturated dissolved hydrogen concentrations that increase with current density.

Effect on cell performance.—Previously, the effect of cathode ionomer on gas crossover was shown. In this section the effect of ionomer content on the cell voltage is investigated. Fig. 5 shows the electrochemical performance of the tested CCMs, namely the cell voltage as well as HFR and *iR*-free cell voltage, which are plotted against

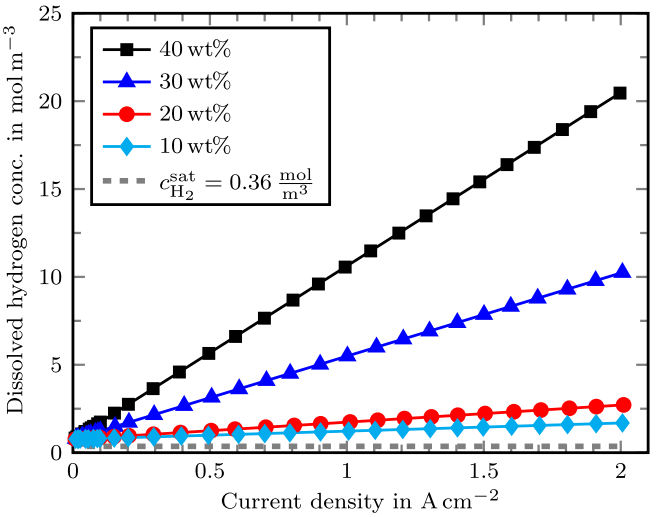

Figure 4. The supersaturated dissolved hydrogen concentration $c^{\star}_{H_2}$ of the different CCMs, which was calculated by Eq. 3 and the determined mass transfer coefficients k^c_l of Fig. 3b. Additionally, the saturated hydrogen concentration $c^{sat}_{H_2}$ (gray, dashed line) is plotted, which correspond to operating conditions: 80°C and atmospheric pressure.

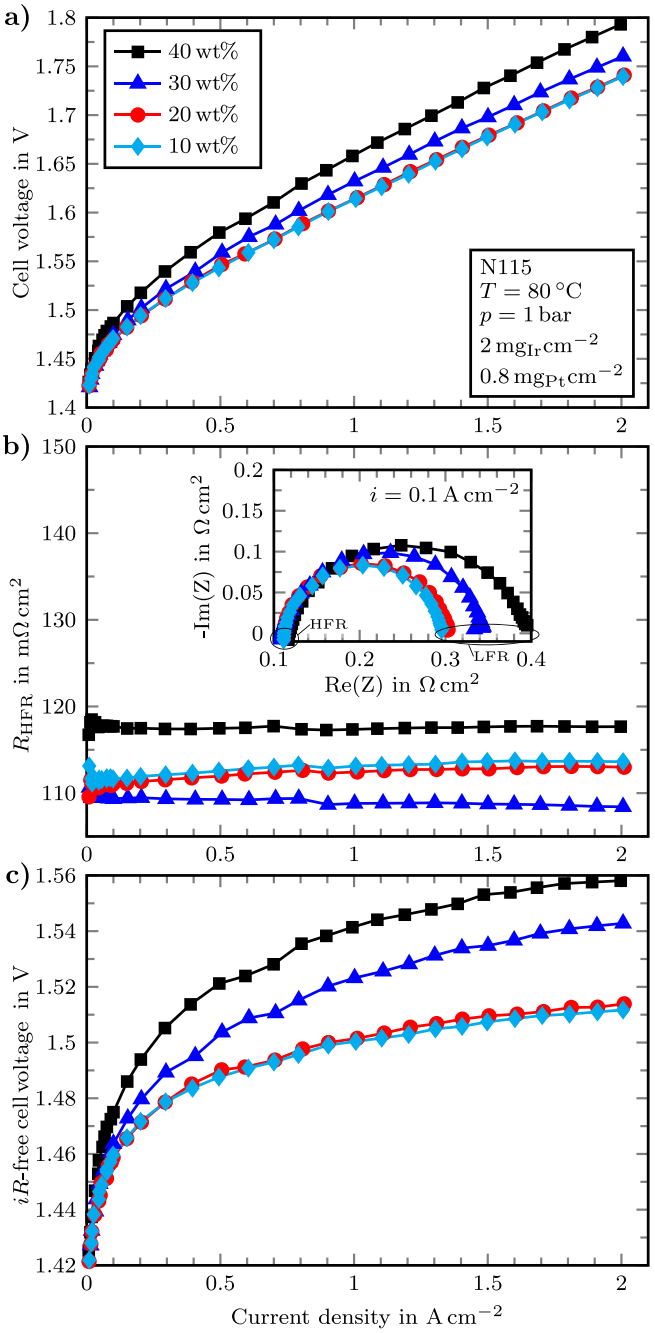

Figure 5. Performance comparison for the different CCMs: a) cell voltage, b) HFR and c) *iR*-free cell voltage plotted versus the applied current density. The inset in b) is a Nyquist plot at 0.1 A cm^{-2}. The high ionomer contents show significantly higher voltages, which also remain in the *iR*-free cell voltage.

current density. In Fig. 5a the polarization curves are shown. CCMs with high ionomer contents (30 and 40 wt%) show higher cell voltages than the CCMs with lower ionomer contents (10 and 20 wt%), for which the polarization curves are quite similar.

In Fig. 5b the HFRs of all CCMs are shown. The measured HFR is not significantly influenced by the variation of cathodic ionomer content. There is no clear visible trend. Furthermore, the differences between the CCMs are small (<10 mΩ cm^2). The major part of the HFR should come from the N115 membrane. The anode system is not changed and the resistances of the catalyst layers are not included within the HFR. Therefore, only the different cathodic catalyst layer-PTL interfaces could lead to changes in HFR, but no hints are visible in this direction.

The inset of Fig. 5b shows Nyquist plots for each CCM at a current density of 0.1 A cm^{-2}. The Nyquist plot shows that the measured impedance data depicts no perfect semicircles (each of the semi arcs is flatter than wide). It can be seen that the HFR is very similar for each CCM, whereas the low frequency resistance (LFR) is higher for the CCMs with higher ionomer contents. This is in perfect agreement with the resistance values obtained from the slopes of the polarization curves (s. Fig. 5a).

The *iR*-free cell voltage profiles are shown in Fig. 5c, which can be calculated by subtracting the ohmic losses ($i \cdot R_{HFR}$) from the cell voltage. It can be seen that the voltage differences between the CCMs, which were observed in the cell voltage (s. Fig. 5a), are still there. Also the *iR*-free cell voltage is higher for the CCMs with higher cathode ionomer contents (30 and 40 wt%) than for the CCMs with lower ionomer contents (10 and 20 wt%). Consequently, the differences in cell voltage are not caused by ohmic losses (membrane or contact), but rather by losses, which have their origin directly within the cathode catalyst layer (e.g. mass and proton transport losses). The origin of these voltage differences are investigate in more detail in the following paragraphs.

Since the anode was kept constant, the differences of the *iR*-free cell voltage may be caused by losses on the cathode side, such as ohmic losses within the catalyst layers and mass transport losses. It is not trivial to analyze the remaining losses without further detailed experiments or models. However, due to the measured H_2 in O_2 content and the calculated supersaturated concentration of dissolved hydrogen (s. Fig. 4) the losses due to cathodic mass transport can be estimated. Therefore, it is assumed that the mass transport losses can be calculated by the Nernst Equation 4, without considering the effects on kinetic and affected proton transport. Consequently, the supersaturated hydrogen concentrations lead to increases in the cathodic half-cell potential ΔE^{c}_{conc} that are considered by the concentration dependence of the Nernst Eq. 4 for the cathodic half-cell:

$$\Delta E^{c}_{conc} = \frac{RT}{2F} \ln\left(\frac{c^{\star}_{H_2}}{c^{ref}_{H_2}}\right) \quad [4]$$

where $c^{ref}_{H_2}$ is chosen to be equal to the saturation concentration $c^{sat}_{H_2}$ of 0.36 mol m^{-3}. So, the increase of the cathodic half-cell potential ΔE^{c}_{conc} can be calculated by Eq. 4 and the determined supersaturated hydrogen concentration of the crossover measurement (s. Fig. 4). Fig. 6a shows the typical logarithmic Nernst correlation between the supersaturated hydrogen concentrations shown in Fig. 4 and the half-cell potential. Accordingly, the half-cell potentials are also higher for the CCMs with higher ionomer contents. For example at a current density of 2 A cm^{-2} cell voltage losses between 10 and 50 mV can be attributed to the increased concentration due to mass transfer losses.

Fig. 6b shows the concentration corrected *iR*-free cell voltage, when subtracting the concentration increased cathodic half-cell potential ΔE^{c}_{conc} 4 from the *iR*-free cell voltage. The resulting concentration corrected *iR*-free cell voltage curves agree quite well with each other. For the purpose of comparison, the not corrected *iR*-free cell voltage curves are also plotted with hollow marks in a transparent style. It can be seen that the curves get closer if corrected by the individual mass transport losses. So, it can be suggested that the voltage differences mainly come from the changes in cathodic half-cell potential that are caused by supersaturated hydrogen concentrations due to different mass transfer resistances of the CCMs with varied cathodic ionomer content.

In a last step, the reaction kinetic parameters for the sluggish oxygen evolution reaction (OER) should be discussed. For this purpose, the Tafel Equation 5 is fitted to the *iR*-free cell voltage at low current densities (in this work: 0.01 to 0.1 A cm^{-2}). For this low current density range it is assumed that all other losses i) mass transport losses, ii) ohmic losses within the catalyst layer and iii) the activation losses of the fast hydrogen evolution reaction can be neglected. Consequently, the increase of the *iR*-free cell voltage within the low current density

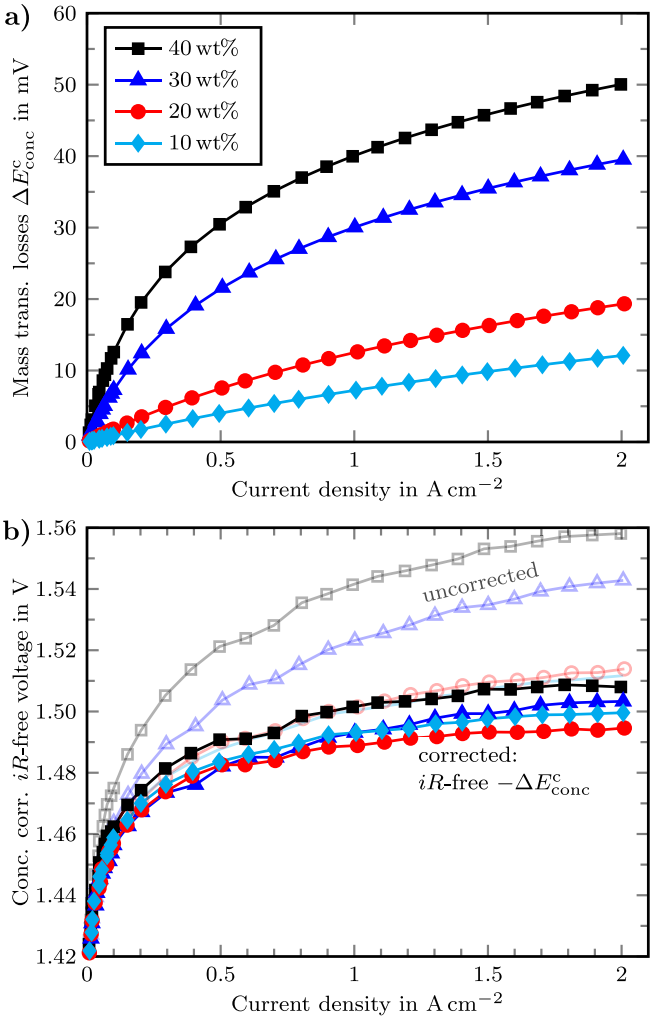

Figure 6. Subfigure a) shows the concentration overpotentials/mass transport losses calculated by Eq. 4 and b) shows the corrected *iR*-free cell voltage by the concentration overpotential plotted against current density. The transparent curves with hollow marks of b) are the original/uncorrected *iR*-free cell voltage curves of Fig. 5c.

range is only caused by the anodic activation overvoltage.

$$\eta = b \ln\left(\frac{i}{i_0}\right) \quad [5]$$

The results of this Tafel analysis are shown in Fig. 7 as dashed lines for each CCM and the corresponding Tafel slopes are shown in the text boxes of Fig. 7. For the common *iR*-free cell voltage curves (not corrected by the shift in cathodic half-cell potential) the results are shown in Fig. 7a. The CCMs with low ionomer contents reveal Tafel slopes of 36–37 mVdec^{-1}, whereas the CCMs with 30 and 40 wt% show significantly higher Tafel slopes of 43 and 47 mVdec^{-1}, respectively. Within literature both Tafel slopes are reported: Mazur et al.[21] measured Tafel slopes of 38.9 mVdec^{-1} for IrO_2 and 34.6−49.5 mVdec^{-1} for IrO_2 supported by TiO_2 by using the thin-film method on a glassy carbon RDE in 0.5 M H_2SO_4 at room temperature and Bernt and Gasteiger [17] measured Tafel slopes within an electrolysis cell of 45−47 mVdec^{-1} for a TiO_2 supported IrO_2 anode catalyst.

Beside the different cathode catalyst layers with varied ionomer contents, identical anode catalyst layers, porous transport layers as well as membranes are used. Consequently, the different Tafel slopes can only be caused by the different cathodic catalyst layers. Since the Pt loading was also identical, the difference has to come from the concentration overpotentials. Consequently, the previously mentioned

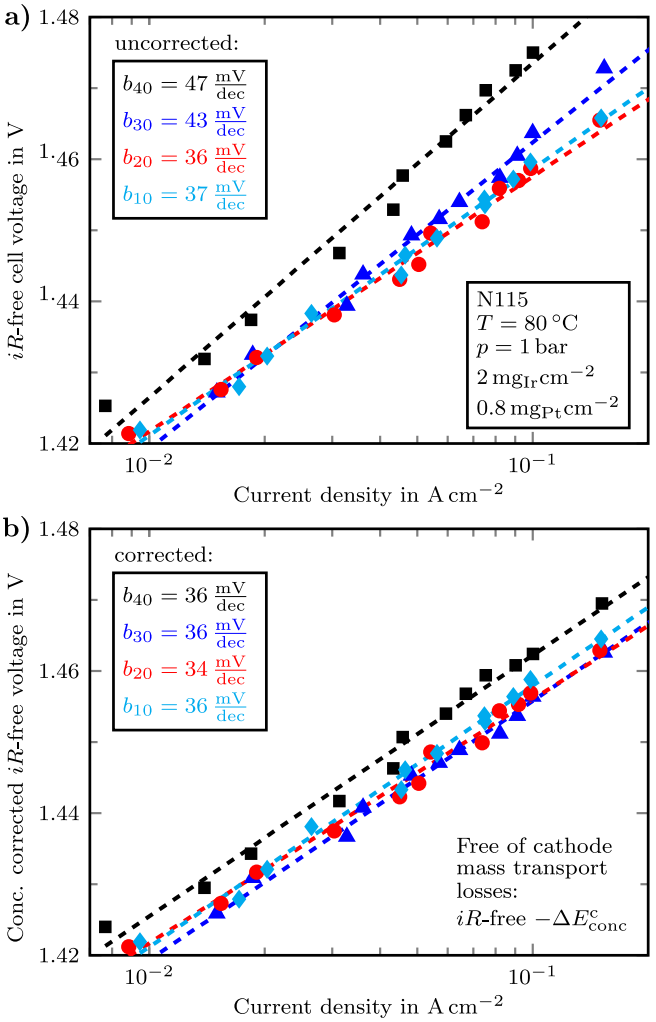

Figure 7. Comparison of the Tafel analysis with a) common *iR*-free cell voltage curves (uncorrected) and b) concentration corrected *iR*-free cell voltage curves for the different ionomer contents 10-40 wt%. The dashed lines are the fitted results of the Tafel analysis, the corresponding Tafel slopes are given in the text boxes. The Tafel analysis is more homogeneous when the *iR*-free cell voltage is also reduced by the cathode mass transport losses.

assumptions (negligible other losses in the low current density range) are not fulfilled for the Tafel analysis. Hence, the different cathodic ionomer contents affect also the cell performance at low current densities, which could be erroneously mapped with the Tafel analyzes on the sluggish OER. Therefore, the Tafel analysis is also performed for the concentration corrected *iR*-free cell voltage. This analysis is shown in Fig. 7b. The Tafel slopes of each CCM are reduced to values around 36 mVdec^{-1} and agree now very well to each. So, the mass transport losses due to hydrogen supersaturation can also affect the low current density range of 0.01 till 0.1 A cm^{-2} and hence affect the Tafel analysis.

Effect of mass transfer resistances on crossover and cell voltage.—The previously shown effects of the cathode ionomer content on hydrogen crossover and cell voltage are summarized in Fig. 8. Therefore, all important values are plotted versus the cathode ionomer content for 3 different current densities. Fig. 8a shows the reduction of the determined mass transfer coefficient with increasing ionomer content. This was mainly explained by i) increases in the average ionomer path way from catalyst toward pore space and ii) reduction in volume specific surface of the ionomer. By definition, the reduction of the mass transfer coefficient means an increase in mass transfer resistances. Consequently, the dissolved hydrogen concentration increases with ionomer content (Fig. 8b). The supersaturated dissolved hydrogen concentration has negative effects on hydrogen crossover (Fig. 8c) and cell voltage (Fig. 8d). The crossover increases due to higher concentration gradients (Fick's law) and the cell voltage increases because of the higher cathode half-cell potential (Nernst equation, increased mass transport losses).

So, for the observed range of the cathode ionomer content (10 to 40 wt%), the crossover and cell voltage increase with increasing ionomer content. Bernt and Gasteiger[17] varied the ionomer content of the PEM water electrolyzer anode. With regard to cell voltage, they show similar results in comparison to this work. The *iR*-free cell voltage increases with increasing anode ionomer contents in the range of 11.6 to 28 wt%. Considering the above presented findings this might be due to the increased supersaturation of dissolved oxygen, because of higher mass transfer resistances and thus increased anode half-cell potential. However, on the anode side also the transport of water could be hindered by increased ionomer contents. So, the experimental findings of Bernt and Gasteiger[17] can be supported by this work. However, Bernt and Gasteiger[17] also show that the *iR*-free cell voltage increases again at very low ionomer contents. They explained this by higher proton resistances within the catalyst layer with less ionomer and consequently higher voltage losses at very low ionomer contents. The optimal ionomer content for their anode catalyst layers were at 11.6 wt% ionomer. So, this agrees very good to the trend of this work, in which the optimal ionomer should be close to 10 wt%. However, the findings of this work should be understood as qualitative results that show the correlation between mass transport resistances and crossover as well as cell voltage.

The fact that the cell voltage increases again at low ionomer contents, because of increased proton transort resistances,[17] should result in a shifting of the reaction front/evolution rate towards the membrane. This could lead to higher supersaturation concentrations directly at the membrane/catalyst layer interface. Consequently, we assume that also the gas crossover should increase again with decreasing ionomer contents.

Conclusions

In this work the ionomer content of PEM water electrolysis cathodes was varied in order to investigate its influence on hydrogen crossover and cell performance. An increase in cathodic ionomer content leads to increases in hydrogen crossover and cell voltage within the investigated ionomer range. Both effects can be entirely explained by the supersaturation of dissolved hydrogen.

It is shown that the determined supersaturated hydrogen concentrations of the crossover experiments are in the right order of magnitude to explain the differences in cell voltage. The supersaturation of dissolved hydrogen enhances the crossover due to the higher concentration gradients across the membrane, which are the driving force for diffusion. The cell voltage is higher because of the increase in cathodic half-cell potential with increasing hydrogen concentration, which can be calculated by using the Nernst equation. In summary, mass transfer resistances within catalyst layers cause supersaturated concentrations of dissolved gases that lead to increases in crossover and cell voltage. This should also occur on the anode side.

These findings highlight the importance of catalyst layer structure. Not only in the context of electrochemical activity, but also related to reduction of mass transfer resistances, which reduce the supersaturation and thus improve the cell performance as well as decrease the crossover. The ionomer content is one key parameter, but there are several others (e.g. catalyst loading), which could be changed to reduce the electrode mass transfer resistance of catalyst layers. It is important to investigate the different mass transport/transfer steps in more detail for systematic development of improved catalyst layers.

Additionally, the *iR*-free cell voltage is often used to obtain kinetic parameters of the anode (Tafel analysis). However, these obtained kinetic parameters are still distorted by mass transport losses, which are caused due to supersaturated dissolved gas concentrations. Even if the Tafel analysis is carried out at low current densities, there are small

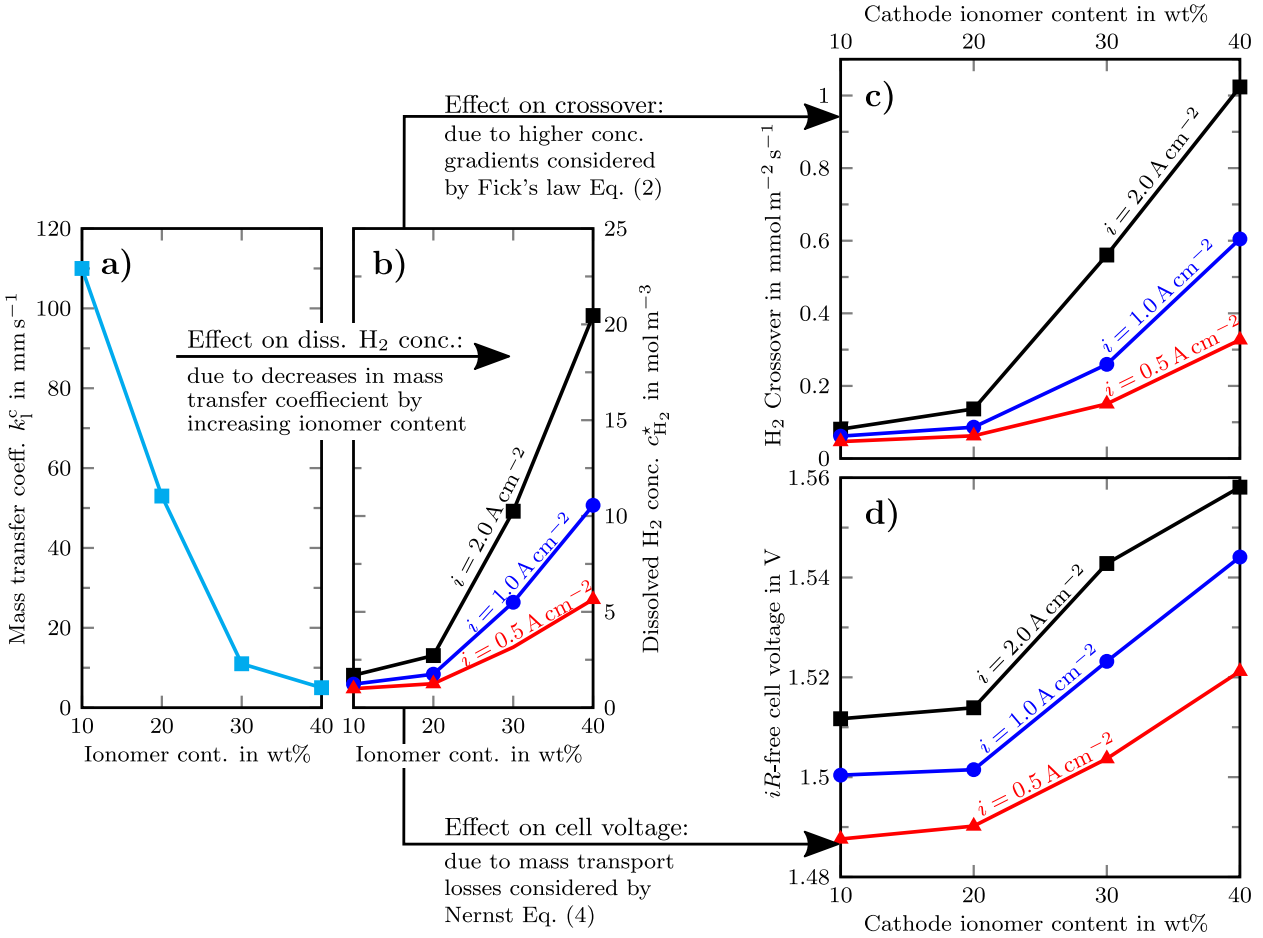

Figure 8. Effect of mass transfer resistances on hydrogen crossover and cell voltage by variation of the cathode ionomer content. The reduced mass transfer coefficient with increasing ionomer content a) leads to highly supersaturated dissolved hydrogen concentrations at high ionomer contents b) that cause increases in hydrogen crossover fluxes c) and cell voltages d).

changes in the half-cell potentials, which should be subtracted. Otherwise the determined kinetic parameters are not free of mass transport effects. These mass transport voltage losses can be obtained by the measurement of gas crossover. So, this can therefore be used to elucidate mass transport losses and contribute to a comprehensive overview of overvoltage sources.

Acknowledgments

The authors thank Daniel Holtz for developing and performing the CCM fabrication method, and Andreas Everwand for performing SEM/EDS measurements, and Michel Süermann and Chrstioph Immerz for fruitful discussions. The authors gratefully acknowledge the financial support by the Federal Ministry of Education and Research of Germany in the framework of PowerMEE (project number 03SF0536B).

ORCID

P. Trinke https://orcid.org/0000-0002-0935-5321
B. Bensmann https://orcid.org/0000-0001-8685-7192

References

1. S. A. Grigoriev, P. Millet, S. V. Korobtsev, V. I. Porembskiy, M. Pepic, C. Etievant, C. Puyenchet, and V. N. Fateev, *Int. J. Hydrogen Energ.*, **34**(14), 5986 (2009).
2. M. Schalenbach, *Int. J. Hydrogen Energ.*, **41**(1), 729 (2016).
3. P. Trinke, B. Bensmann, and R. Hanke-Rauschenbach, *Int. J. Hydrogen Energ.*, **42**(21), 14355 (2017).
4. P. Trinke, P. Haug, J. Brauns, B. Bensmann, R. Hanke-Rauschenbach, and T. Turek, *J. Electrochem. Soc.*, **165**(7), F502 (2018).
5. M. Inaba, T. Kinumoto, M. Kiriake, R. Umebayashi, A. Tasaka, and Z. Ogumi, *Electrochim. Acta*, **51**(26), 5746 (2006).
6. H. Ito, T. Maeda, A. Nakano, and H. Takenaka, *Int. J. Hydrogen Energ.*, **36**(17), 10527 (2011).
7. P. Trinke, B. Bensmann, S. Reichstein, R. Hanke-Rauschenbach, and K. Sundmacher, *J. Electrochem. Soc.*, **163**(11), F3164 (2016).
8. F. Barbir, *Sol. Energ.*, **78**(5), 661 (2005).
9. S. S. Kocha, J. Deliang Yang, and J. S. Yi, *AIChE J.*, **52**(5), 1916 (2006).
10. D. Ye, Z. Tu, Y. Yu, Y. Cai, H. Zhang, Z. Zhan, and M. Pan, *Int. J. Energ. Res.*, **38**(9), 1181 (2014).
11. M. Schalenbach, T. Hoefner, P. Paciok, M. Carmo, W. Lueke, and D. Stolten, *J. Phys. Chem. C*, **119**(45), 25145 (2015).
12. P. Trinke, B. Bensmann, and R. Hanke-Rauschenbach, *Electrochem. Commun.*, **82**, 98 (2017).
13. K. Kikuchi, Y. Tanaka, Y. Saihara, M. Maeda, M. Kawamura, and Z. Ogumi, *J. Colloid Interf. Sci.*, **298**(2), 914 (2006).
14. K. Kikuchi, A. Ioka, T. Oku, Y. Tanaka, Y. Saihara, and Z. Ogumi, *J. Colloid Interf. Sci.*, **329**(2), 306 (2009).
15. H. Matsushima, D. Kiuchi, and Y. Fukunaka, *Electrochim. Acta*, **54**(24), 5858 (2009).
16. F. Hegge, R. Moroni, P. Trinke, B. Bensmann, R. Hanke-Rauschenbach, S. Thiele, and S. Vierrath, *J. Power Sources*, **393**, 62 (2018).
17. M. Bernt and H. A. Gasteiger, *J. Electrochem. Soc.*, **163**(11), F3179 (2016).
18. C. L. Young (Ed.), *Hydrogen and deuterium*, Vol. 5/6 of Solubility data series, Pergamon Press, Oxford, 1981.
19. A. Z. Weber and J. Newman, *J. Electrochem. Soc.*, **151**(2), A311 (2004).
20. D. R. Stull, *Ind. Eng. Chem.*, **39**(4), 517 (1947).
21. P. Mazúr, J. Polonský, M. Paidar, and K. Bouzek, *Int. J. Hydrogen Energ.*, **37**(17), 12081 (2012).